High-Level Rovibrational Calculations on Ketenimine

Martin Tschöpe[†], Benjamin Schröder[†], Sebastian Erfort[†] and Guntram Rauhut[*]

Institute for Theoretical Chemistry, University of Stuttgart, Stuttgart, Germany

From an astrochemical point of view ketenimine (CH_2CNH) is a complex organic molecule (COM) and therefore likely to be a building block for biologically relevant molecules. Since it has been detected in the star-forming region Sagittarius B2(N), it is of high relevance in this field. Although experimental data are available for certain bands, for some energy ranges such as above 1200 cm^{-1} reliable data virtually do not exist. In addition, high-level *ab initio* calculations are neither reported for ketenimine nor for one of its deuterated isotopologues. In this paper, we provide for the first time data from accurate quantum chemical calculations and a thorough analysis of the full rovibrational spectrum. Based on high-level potential energy surfaces obtained from explicitly correlated coupled-cluster calculations including up to 4-mode coupling terms, the (ro)vibrational spectrum of ketenimine has been studied in detail by variational calculations relying on rovibrational configuration interaction (RVCI) theory. Strong Fermi resonances were found for all isotopologues. Rovibrational infrared intensities have been obtained from dipole moment surfaces determined from the distinguishable cluster approximation. A comparison of the spectra of the CH_2CNH molecule with experimental data validates our results, but also reveals new insight about the system, which shows very strong Coriolis coupling effects.

Keywords: ketenimine, *ab initio* calculations, Fermi resonances, rotational spectrum, VSCF/VCI theory, rovibrational calculations

1. INTRODUCTION

More than 200 molecules have been detected in the interstellar medium (ISM) or circumstellar shells (Müller et al., 2001, 2005; Endres et al., 2016; McGuire, 2018) presenting a chemical variety from rather stable to highly reactive species such as radicals, carbenes, and molecular ions. In a similar way, the size measured by the number of atoms varies substantially from simple diatomics (e.g., CO, CN, and OH; Weinreb et al., 1963; Jefferts et al., 1970; Wilson et al., 1970), to carbon-chain molecular species like cyanopolyynes (HC_nN; Ohishi and Kaifu, 1998) and simple organic molecules like methanol (CH_3OH; Ball et al., 1970), up to still larger compounds like polycyclic aromatic hydrocarbons (PAHs; Allamandola et al., 1989) and fullerenes (C_{60}; Cami et al., 2010). Within the context of astrochemistry molecules with 6 or more atoms are usually referred to as complex molecules and when carbon is present also as complex *organic* molecules (COMs; Herbst and van Dishoeck, 2009). Such compounds are thought to be important building blocks for biologically relevant molecules (Woon, 2002; Theule et al., 2011; Ohishi, 2019) and accordingly, much attention has been paid to the study of formation pathways for COMs (Herbst and van Dishoeck, 2009; Öberg, 2016, and references therein).

Examples of such COMs are the class of imines (R-C=NH). They have been shown to be important intermediates for the hydrogenation of CN moieties (Theule et al., 2011; Krim et al., 2019). Recently, formation of imines has been reported for radiative-processing of ices. Vasconcelos et al. investigated the products from ion irradiation of N_2-CH_4 ice mixtures by *in-situ* Fourier transform infrared spectroscopy (FTIR) and, among others, methyleneimine was identified (Vasconcelos et al., 2020). In a similar fashion, Carvalho and Pilling (2020) detected ketenimine by FTIR spectroscopy upon irradiation of acetonitrile ice with X-rays (6–2000 eV). Ketenimine ($H_2C=C=NH$) is one of only 4 imines which have been conclusively identified to be present in the ISM (Godfrey et al., 1973; Kawaguchi et al., 1992; Lovas et al., 2006; Zaleski et al., 2013). Using the 100 m Green Bank Telescope Lovas and coworkers observed three rotational transitions of ketenimine toward the star-forming region Sagittarius B2(N) (Lovas et al., 2006). It is known that temperatures in Sagittarius B2(N) vary between 40 K in the envelope and 300 K in the hot dense core (Martín-Pintado et al., 1996). Therefore, it could be possible that not only the rotational spectrum of ketenimine can be detected with radio telescopes, but also the rovibrational spectrum due to IR spectroscopy. Since Sagittarius B2(N) is a star forming region, the question arises whether ketenimine can be found in protoplanetary disks or even exoplanet atmospheres. Considering the recent successes in this field (Charbonneau et al., 2002; Mandell et al., 2013; Gandhi et al., 2020) as well as the upcoming space telescopes James Webb Space Telescope (JWST) and Atmospheric Remote-sensing Infrared Exoplanet Large-survey (ARIEL) with high sensitivity in this spectral range this is a feasible aim.

Given its importance as the simplest member of a larger class of chemically interesting molecules (Alajarin et al., 2012), ketenimine has been subject to a number of experimental spectroscopic investigations which revealed a complex rovibrational spectrum. The first spectroscopic investigation of ketenimine was reported by Jacox and Milligan (1963). Infrared transitions of the transient species were tentatively assigned following the reaction of NH with acetylene in argon matrix. The assignment was later confirmed and extended by Jacox (1979) in an argon matrix-isolation study of the photoisomerization of acetonitrile.

A gas phase rotational spectrum of ketenimine was obtained by Rodler and coworkers using microwave spectroscopy (Rodler et al., 1984). Ground-state rotational parameters of $A_0 = 201443.69$, $B_0 = 9663.138$, and $C_0 = 9470.127$ MHz were determined from a fit to Watson's S-reduced rotational Hamiltonian (Watson, 1977) in the I^r representation. The latter parameters show that ketenimine is a near-prolate asymmetric top (asymmetry parameter $\kappa = -0.998$). Measurements of Stark-splittings (Rodler et al., 1984) yielded the ground state dipole moments $^a\mu_0 = 0.431(1)$ D and $^c\mu_0 = 1.371(6)$ D. Rodler et al. later carried out a high-resolution analysis in the 4–7 GHz region for the main as well as the ND isotopologue revealing small splittings in the former case, due to the imino inversion (Rodler et al., 1986). The latest study of the vibrational ground state rotational spectrum of ketenimine was performed by Degli Esposti at submillimeter wavelength (Degli Esposti

et al., 2014). In total, 297 line frequencies were analyzed yielding spectroscopic parameters that allow for the accurate prediction of rotational transitions up to 1 THz.

The rovibrational spectrum of ketenimine has been studied by both, in low-resolution (August, 1986) as well as high-resolution (Ito et al., 1990; Ito and Nakanaga, 2010; Bane et al., 2011a,b,c). A gas phase spectrum of the $\tilde{\nu}_3 = 2044$ cm^{-1} CCN-stretching vibration has been obtained by Ito et al. (1990) using FTIR spectroscopy. Analysis of the spectrum revealed a complicated structure due to several Coriolis-type interactions, which could only be analyzed approximately due to missing information on the perturbing states. Almost 20 years later Ito and Nakanaga reported the observation of the CNH bending rovibrational spectrum around $\tilde{\nu}_6 = 1000$ cm^{-1} using FTIR spectroscopy. Again, strong Coriolis perturbations precluded a detailed analysis of the ν_6 state and only effective spectroscopic parameters for individual K_a sub-bands were obtained. The latter values allowed the ν_{10} (CH_2 rocking) and ν_{11} (torsion) vibrations to be identified as likely perturbers, based on their large contribution to the vibration-rotation interaction constant α_6^A.

In a series of articles Bane and coworkers presented a thorough experimental analysis of the low lying fundamental bands of ketenimine (Bane et al., 2011a,b,c). The observed bands encompass the out-of-plane and in-plane CCN bending vibrations around $\tilde{\nu}_{12} = 409$ and $\tilde{\nu}_8 = 466$ cm^{-1} (Bane et al., 2011c), respectively, the CH_2 wagging mode ($\tilde{\nu}_7 = 693$ cm^{-1}; Bane et al., 2011b) and the CH_2 rocking mode ($\tilde{\nu}_{10} = 983$ cm^{-1}) as well as the strong CNH bending mode ν_6 (Bane et al., 2011a). Following the assignment of more than 6,000 rovibrational transitions and fitting of the spectrum, an intricate system of Coriolis-coupled states was revealed whereby all 5 observed states are coupled via Coriolis-coupling either directly (e.g., a-axis Coriolis coupled ν_{12} & ν_8) or indirectly. The analysis required the inclusion of unobserved "dark states" $2\nu_8$, $\nu_8 + \nu_{12}$, and $2\nu_{12}$ which are also expected to be strongly Coriolis-coupled amongst themselves. While the global fit to Watson's S-reduced Hamiltonian (I^r) reproduced the observed rovibrational transition frequencies, Bane et al. noted that the torsion fundamental ν_{11} around 880 cm^{-1} probably also adds to the complex rovibrational coupling but considered inclusion of this interaction intractable.

Theoretical work on the rotational and rovibrational spectroscopy of ketenimine is rather scarce and either based on limited *ab initio* methods (Kaneti and Nguyen, 1982; Brown et al., 1985) or has been done only in support of dedicated experimental investigations (Ito et al., 1990; Ito and Nakanaga, 2010; Bane et al., 2011c). In the latter case, the work of Bane and coworkers (Bane et al., 2011c) provided the previously most accurate predictions of the fundamental frequencies with a root-mean-squared deviation of 11 cm^{-1}. The results were obtained from B3LYP/cc-pVTZ harmonic frequencies which were uniformly scaled by a factor of 0.965. Given its possible importance in astrochemical reaction networks and the strong rovibrational couplings a more in-depth look at the rotational and rovibrational spectroscopy of ketenimine appears desirable.

Recently, some of us reported on the implementation of a new program for variational rovibrational calculations within the

MOLPRO package of *ab initio* programs (Erfort et al., 2020a). The approach combines the well established MOLPRO capabilities (Werner et al., 2020) of obtaining multidimensional potential energy and dipole moment surfaces, comprehensive symmetry information and the accurate determination of vibrational wave functions with efficient calculation of partition functions, rovibrational transition frequencies, and transition dipole matrix elements in an almost black-box manner. Within this study here, we report about high-level *ab initio* calculations based on anharmonic potential energy surfaces obtained from explicitly correlated coupled-cluster theory, which allows for a detailed analysis of the (ro)vibrational spectra of the title compound. Compared to previous work the rovibrational calculations have been extended by pure rotational spectra, which is a newly implemented feature in MOLPRO.

2. COMPUTATIONAL DETAILS

Geometries, harmonic frequencies and normal coordinates of ketenimine (X^1A') and its C_s symmetric isotopologues were computed at the level of frozen-core explicitly correlated coupled-cluster theory, CCSD(T)-F12b, in combination with a basis set of triple-ζ quality, i.e., cc-pVTZ-F12 (Adler et al., 2007). Hartree-Fock energies were corrected by addition of the complementary auxiliary basis set singles correction (CABS) (Knizia and Werner, 2008).

n-mode expansions of the potential energy surface (PES) and the dipole moment surface (DMS) being truncated after 4th order were used in all calculations (Ziegler and Rauhut, 2018). A multi-level scheme has been employed throughout (Pflüger et al., 2005; Yagi et al., 2007), in which the 1D and 2D terms of the PES were computed at the CCSD(T)-F12b/cc-pVTZ-F12 level, while the explicitly correlated distinguishable clusters approach, DCSD-F12b, in combination with a smaller cc-pVDZ-F12 basis was used for the 3D and 4D terms. The 1D and 2D terms of the DMS were computed at the conventional DCSD/cc-pVTZ-F12 level and the 3D and 4D terms at the DCSD/cc-pVDZ-F12 level (Kats and Manby, 2013; Kats et al., 2015). In total about 170,000 *ab initio* points were used for representing the surfaces. Efficient Kronecker product fitting was employed to transform this grid representation into an analytical one consisting of 10 local B-splines per dimension (Ziegler and Rauhut, 2016).

Vibrational self-consistent field theory (VSCF) has been used to determine one-mode wavefunctions (modals) based on the Watson Hamiltonian (Watson, 1968). Vibrational angular momentum terms (VAM) were not included within the variational determination of the modals, but were added *a posteriori* to the state energies (Neff et al., 2011). A mode-dependent basis of 20 distributed Gaussians has been used throughout for representing the modals. Subsequent state-specific configuration-selective vibrational configuration interaction calculations (VCI) were used for calculating accurate state energies (Neff and Rauhut, 2009). The correlation space contained single to 6-tuple excitations up to the 8th root per mode and a maximum sum of quantum numbers of 15. This resulted in about $4 \cdot 10^6$ Hartree products (configurations)

per irreducible representation. These calculations included VAM terms based on a constant $\boldsymbol{\mu}$-tensor. Eigenvalues were determined with our residuum based eigenvalue solver (RACE) (Petrenko and Rauhut, 2017).

Within the calculation of the rovibrational spectra we also use the Watson-operator (Watson, 1968)

$$H_{\text{Watson}} = \frac{1}{2} \sum_{\alpha\beta} J_\alpha \mu_{\alpha\beta} J_\beta - \frac{1}{2} \sum_{\alpha\beta} (J_\alpha \mu_{\alpha\beta} \pi_\beta + \pi_\alpha \mu_{\alpha\beta} J_\beta) + H_{\text{Vib}},$$

(1)

where J_α denotes the total angular momentum operator, π_α the vibrational angular momentum operator and $\mu_{\alpha\beta}$ refers to an element of the inverse effective moment of inertia tensor. The summations over α and β run over the three molecule fixed Cartesian space coordinates. The first term in Equation (1) gives the kinetic energy of rotational motion and the second term couples rotation and vibration and is referred to as Coriolis term. All other terms of the Watson Hamiltonian are purely vibrational operators and are thus summarized in the term denoted H_{Vib}. Within rovibrational configuration interaction (RVCI) theory the rovibrational wave functions are expanded in terms of products of VCI wave functions and rotational basis functions (Erfort et al., 2020a,b). The latter can be either primitive symmetric top eigenfunctions or Wang combinations of symmetric top functions (Wang, 1929; Špirko et al., 1985).

In the following, we will distinguish between rotational configuration interaction (RCI) and rovibrational configuration interaction (RVCI). RCI is an approximation, in which no rovibrational interaction between different vibrational states is considered. This corresponds to neglecting the second term, see Equation (1), as well as all terms off-diagonal in the vibrational quantum numbers, arising from the 1D and higher order expansion of the $\boldsymbol{\mu}$-tensor (centrifugal distortion). Since every RCI-matrix is thus constructed for a single VCI wave function, the vibrational state identity can be trivially assigned for every rovibrational state. In contrast, within RVCI all rovibrational interactions are considered. As a consequence the only "good" quantum number is the angular momentum quantum number J and the parity of the rovibrational state. In this sense, RVCI yields the physically meaningful results. However, we found that a comparison of RVCI with the RCI results is helpful to understand and visualize both the effects of Coriolis interaction and intensity borrowing mechanisms in general. Again, it shall be noted that for comparison with experiments only RVCI results should be used.

The rovibrational intensities are calculated according to

$$I = \frac{2\pi^2}{3} \frac{N_A}{\epsilon_0 h^2 c^2} \frac{e^{-E''/k_B T}(1 - e^{-(E'-E'')/k_B T})}{Q(T)} (E' - E'')R^2. \quad (2)$$

In Equation (2), the first two prefactors contain only constants. The next factor corresponds to the thermal distribution function, with the temperature T, Boltzmann constant k_B, the energy of the lower state E'' and the upper state E' as well as the temperature dependent partition function $Q(T)$. For the latter, we use the separability approximation $Q = Q_{\text{vib}} Q_{\text{rot}}$ for several reasons.

First, we are investigating a relatively low temperature regime up to 300 K, where the partition function converges quickly with increasing excitation, such that errors in energies for high-lying states have little influence. Second, we have shown in our previous work (Erfort et al., 2020a), that for H_2CO and H_2CS the differences between experimental $Q(T)$ values and theoretically approximated $Q_{vib}Q_{rot}$ values for the partition function are lower than 2 % up to 300 K. In addition to that, the partition function is the same global factor for every transition and since we are primarily interested in relative intensities rather than in absolute intensities, it is therefore not crucial for us. The last two factors in Equation (2) correspond to the frequency of the transition $(E' - E'')$ and the squared transition moment R^2. The calculation of the latter within RVCI has been outlined previously (Erfort et al., 2020a). For ketenimine all nuclear spin statistical weights show the values of 24.

Further approximations are used to limit the calculation times. First of all, we are not considering hot bands. Due to relatively low temperatures and absence of fundamentals with particularly low energies, these bands have fairly low intensities and are mainly hidden behind significantly more intense transitions arising from the vibrational ground state. This is supported by a comparison to the results of Bane and coworkers (Bane et al., 2011c). Moreover, the inverse effective moment of inertia tensor μ is expanded to the 0th order for the RVCI calculation. Within these computations all fundamental bands, seven combination bands ($\nu_3 + \nu_5$, $\nu_3 + \nu_6$, $\nu_5 + \nu_6$, $\nu_6 + \nu_{10}$, $\nu_7 + \nu_8$, $\nu_7 + \nu_{12}$, and $\nu_8 + \nu_{12}$) and seven overtones ($2\nu_6$, $2\nu_7$, $2\nu_8$, $2\nu_{10}$, $2\nu_{12}$, $3\nu_8$, and $3\nu_{12}$) were simultaneously considered, giving in total $N_{vib} = 27$ vibrational states (including the ground state). As a convergence check we performed a calculation with angular momentum quantum number of $J \leq 70$ and one with $J \leq 100$. The VCI calculations were performed in parallel using 9 cores, with a total computational time of 100 h. The required memory for the subsequent serial RVCI treatment is less than 40 GB. As an example, the RVCI matrix for $J = 70$, with $N_{vib} = 27$ vibrational states is of size $(2J + 1)N_{vib} = 3,807$. Although, this is relatively small in comparison to other rovibrational software, the results are nevertheless very accurate. A possible reason for this lies in the very accurate and compact vibrational basis, in the form of VCI wavefunctions. Computational timings on a single CPU core were about 83 min for RVCI energies and about 14 h for RVCI intensities for $J \leq 70$. For the same upper bound of J there were 3.81×10^7 transitions considered and about 1.41×10^6 of them where found to be significant. For $T = 300$ K the partition function is converged to $Q(T) = 2.05 \times 10^5$ at $J = 71$.

3. RESULTS AND DISCUSSION

3.1. Geometrical Parameters, Rotational Constants, and Dipole Moments

Geometrical parameters of the main ketenimine isotopologue as well as two deuterated variants have been calculated and are provided in **Table 1**. The parameters obtained from the Born-Oppenheimer equilibrium geometry are denoted r_e. The only experimental geometrical parameter available for comparison is a

mixed experimental-theoretical valence angle $\alpha(C_2NH_3)$ (Rodler et al., 1986). From a semi-rigid bender analysis of the $9_{1,8}$-$10_{0,10}$ ground state rotational transition, Rodler and coworkers determined a value of $115.4 \pm 0.6°$ for $\alpha(C_2NH_3)$ which is in excellent agreement with our optimized value of $114.76°$. To account for vibrational effects r_a and r_g parameters have been calculated. While the former correspond to parameters obtained from atomic positions averaged over the VCI ground state wavefunction, the latter are instantaneous inter-nuclear distances calculated from an expectation value of the bond lengths expanded in terms of the normal coordinates. As is typically observed (Czakó et al., 2009; Dinu et al., 2020), both sets of vibrationally averaged bond lengths differ substantially from each other with the largest absolute difference of 0.0169 Å observed for r(NH_3) in the main isotopologue. The CNH angle $\alpha(C_2NH_3)$ shows a slightly larger vibrational effect compared to other angles, in line with the inversion character of this coordinate. The barrier to planarity (C_{2v}) was computed to be 5249 cm^{-1} at the CCSD(T)-F12b/cc-pVTZ-F12 level and is thus too high for tunneling effects in the fundamental modes to be of any importance. The semi-rigid bender analysis (Rodler et al., 1986) yielded a barrier height of 4700±200 cm^{-1} which compares well with the present theoretical result. The imaginary frequency characterizing the transition state amounts to i908 cm^{-1}. Note that there is no stationary point on the potential energy surface for a planar structure of neutral ketenimine.

Calculated and experimental (Rodler et al., 1984, 1986) rotational parameters for ketenimine isotopologues are compared in **Table 2**. There, rotational parameters A, B, and C obtained from the equilibrium geometry are denoted by method r^e. Following the work of Czakó et al. (2009), vibrationally averaged rotational parameters are approximated from the expectation value of the μ-tensor (Watson, 1968) over VCI wavefunctions. An n-mode expansion of the μ-tensor up to 3D terms has been employed in these calculations. Since this approach does not account for Coriolis coupling contributions to the rotational parameters, these are added via a correction based on Vibrational second-order perturbation theory (VPT2) (Rauhut, 2015; Dinu et al., 2020). The final equation for the rotational parameters B_v^α ($\alpha = a, b, c$) within a vibrational state v is thus given by

$$B_v^\alpha \approx \frac{\langle \mu_{\alpha\alpha} \rangle_v}{2} + \sum_k \frac{2(B_e^\alpha)^2}{\omega_k} \sum_l \left(\zeta_{kl}^\alpha\right)^2 \frac{3\omega_k^2 + \omega_l^2}{\omega_k^2 - \omega_l^2} \left(v_k + \frac{1}{2}\right). \quad (3)$$

In Equation (3), $\langle \mu_{\alpha\alpha} \rangle_v$ is the expectation value of a diagonal μ-tensor element evaluated over the VCI wavefunction for state v. In the second term of Equation (3), constituting the VPT2 Coriolis correction, B_e^α is the equilibrium rotational constant with respect to rotation about an axis α, ω_k are harmonic vibrational frequencies and ζ_{kl}^α are Coriolis constants that describe the coupling of vibrations k and l via rotation about the α-axis. Results obtained from Equation (3) for the vibrational ground state are denoted either $\langle \mu_{\alpha\alpha} \rangle_0$ or $\langle \mu_{\alpha\alpha} \rangle_0$+VPT2 in **Table 2**, depending on whether the Coriolis correction is included or not. Notice that in the evaluation of $\langle \mu_{\alpha\alpha} \rangle_v$ the μ-tensor has been expanded up to 3D terms.

TABLE 1 | Computed geometrical parameters of ketenimine and its deuterated isotopologues.

Coord.	r_e	$H_2C=C=NH$		$D_2C=C=ND$		$H_2C=C=ND$	
		r_a	r_g	r_a	r_g	r_a	r_g
$r(C_1H_1)$	1.0791	1.0829	1.0991	1.0823	1.0938	1.0818	1.0992
$r(C_1C_2)$	1.3135	1.3175	1.3205	1.3172	1.3203	1.3173	1.3204
$r(C_2N)$	1.2284	1.2302	1.2335	1.2302	1.2336	1.2303	1.2335
$r(NH_3)$	1.0174	1.0202	1.0371	1.0196	1.0318	1.0211	1.0316
$\alpha(C_2NH_3)$	114.76	115.07		114.95		115.02	
$\alpha(C_1C_2N)$	174.05	174.10		174.08		174.10	
$\alpha(H_1C_1C_2)$	119.88	119.73		119.78		119.75	
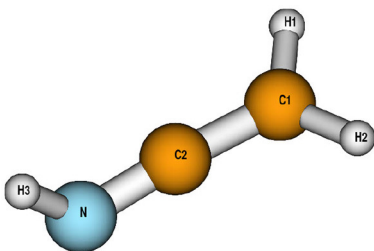
TABLE 2 | Computed and experimental rotational constants in GHz.

Isotopologue	Method	A	B	C
$H_2C=C=NH$	r^e	201.08792 (−0.18%)	9.65878 (−0.05%)	9.47482 (+0.05%)
	$\langle\mu_{\alpha\alpha}\rangle_0$	201.79883 (+0.18%)	9.62993 (−0.34%)	9.43904 (−0.33%)
	$\langle\mu_{\alpha\alpha}\rangle_0$+VPT2	200.31173 (−0.56%)	9.62412 (−0.40%)	9.43309 (−0.39%)
	Exp.[a]	201.44527	9.66315	9.47015
$D_2C=C=ND$	r^e	103.66119	8.05874	7.78830
	$\langle\mu_{\alpha\alpha}\rangle_0$	104.74983	8.03709	7.75996
	$\langle\mu_{\alpha\alpha}\rangle_0$+VPT2	103.35526	8.03232	7.75515
$H_2C=C=ND$	r^e	162.40310 (−0.51%)	9.03436 (+0.02%)	8.96746 (+0.06%)
	$\langle\mu_{\alpha\alpha}\rangle_0$	163.27301 (+0.02%)	9.00356 (−0.33%)	8.93460 (−0.31%)
	$\langle\mu_{\alpha\alpha}\rangle_0$+VPT2	162.21271 (−0.63%)	8.99879 (−0.38%)	8.92979 (−0.36%)
	Exp.[a]	163.24242	9.03295	8.96219

[a]*Values determined from fits to Watson's S-reduced Hamiltonian (Rodler et al., 1984, 1986).*
Where available, percentage deviations of calculated results with respect to experimental data is given in parentheses.

Inspection of **Table 2** shows rather large deviations of the Coriolis-corrected vibrationally averaged rotational parameters of −0.56, −0.40, and −0.39% with respect to experimental results (Rodler et al., 1984, 1986) for A_0, B_0, and C_0, respectively. In contrast, the calculated equilibrium rotational parameters are in much better agreement with the experimental ground state rotational parameters, which is mainly due to error compensation. To confirm this, a geometry optimization at the all-electron CCSD(T)-F12b level of theory in conjunction with a cc-pCVTZ-F12 basis set (Hill et al., 2010) was carried out. This yields equilibrium rotational parameters (in GHz) for the main ketenimine isotopologue of 202.06657, 9.70127, and 9.51561 for A_e, B_e, and C_e, respectively. Adding the corrections due to vibrational averaging and Coriolis-coupling results in $A_0 =$ 201.290 38 GHz (−0.08%), $B_0 =$ 9.666 61 GHz (+0.04%), and $C_0 =$ 9.464 40 GHz (+0.04%), where deviations with respect to the experimental results of Rodler et al. (1984, 1986) are given in parentheses. The agreement of these corrected results with the experimental ones is excellent, but it is well-known that core correlation effects should not be considered without the inclusion of high-level coupled-cluster terms, e.g., CCSDT(Q), at the same time, because they often partly compensate each other (Ruden et al., 2004; Meier et al., 2011; Puzzarini et al., 2020). Moreover, rovibrational intensities as considered below

depend on several quantities and the impact of these additional corrections might be different for the individual quantities. Consequently, there is no unique answer, if the partial inclusion of these corrections will lead to better results. In any case, the inclusion of these high-level corrections is beyond the focus of this study and we neither did account for core correlation effects nor high-order coupled-cluster terms in the calculations presented below.

Experimental high-resolution spectroscopic investigations have revealed strong a-axis Coriolis coupling among the low lying vibrational states of ketenimine, especially for the pair of fundamentals ν_8 and ν_{12} (Bane et al., 2011a,b,c). This can also be shown by comparing rotation-vibration coupling constants α_i^β. From the rotational constants presented by Bane et al. (2011a) α_i^β can be approximated by $\alpha_i^\beta = B_0^\beta - B_i^\beta$. This yields 6185.3, −34.0, and −13.4 MHz for α_{12}^A, α_{12}^B, and α_{12}^C, respectively, and −2845.0, −8.1, and −22.1 MHz for α_8^A, α_8^B, and α_8^C, respectively. These values should be compared to our theoretical VPT2 results of 444.5, −34.2, and −14.7 MHz for α_{12}^A, α_{12}^B, and α_{12}^C, respectively, and 2497.5, −9.3 and −22.7 MHz for α_8^A, α_8^B and α_8^C, respectively. Following Papoušek and Aliev (1982), the latter values have been corrected for the a-axis Coriolis resonance between ν_{12} and ν_8 in order to be comparable with the results of Bane and coworkers.

TABLE 3 | Calculated dipole moments $\vec{\mu}$ (in D) of ketenimine and its deuterated isotopologues.

Isotopologue	$\bar{\mu}_e$			$\bar{\mu}_0$		
	$^a\mu_e$	$^c\mu_e$	$\|\bar{\mu}_e\|$	$^a\mu_0$	$^c\mu_0$	$\|\bar{\mu}_0\|$
$H_2C=C=NH^a$	0.5008	1.4056	1.4912	0.4587	1.3766	1.4510
$H_2C=C=ND$	0.4643	1.4170	1.4912	0.4314	1.4028	1.4676
$D_2C=C=ND$	0.4669	1.4162	1.4912	0.4394	1.3940	1.4616

^{a}Experimental results (Rodler et al., 1984): $^a\mu_0 = 0.434(1)$, $^c\mu_0 = 1.371(6)$, and $\|\bar{\mu}_0\| = 1.438(6)$ D.

To this end, the corresponding $(i, j) = (12, 8)$ or $(8, 12)$ term in the Coriolis contribution to α_i^β (cf. second term in Equation 3) is replaced according to

$$(\zeta_{ij}^\beta)^2 \frac{3\omega_i^2 + \omega_j^2}{\omega_i^2 - \omega_j^2} \rightarrow -(\zeta_{ij}^\beta)^2 \frac{B_e^\beta (\omega_i - \omega_j)^2}{\omega_i \omega_j (\omega_i + \omega_j)}.$$

We have also investigated whether symmetry allowed off-diagonal contributions α_k^{AC} are important for ketenimine, following the work of Aliev and Watson (1985), but found their contribution to effective $\tilde{\alpha}_{12}^\beta$ and $\tilde{\alpha}_8^\beta$ after diagonalization of the respective $B_i^{\alpha\beta}$ matrices negligible.

While the B and C components are in excellent agreement between experiment and theory, the A components show large differences. Moreover, the differences between experiment and theory for ν_{12} and ν_8 are almost identical but of opposite sign (-5740.8 MHz for ν_{12} and 5342.5 MHz for ν_8). For comparison, not accounting for Coriolis resonance yields unphysical VPT2 values of -59021.2 and 61996.7 MHz for α_8^A and α_{12}^A, respectively. Such effects are unambiguous indications of strong Coriolis coupling. The preceding discussion clearly shows that a simple treatment of the rotational problem and the rovibrational couplings in ketenimine, based on e.g., Equation (3) or VPT2, has to proceed with caution. A variational treatment employing the exact rovibrational Hamiltonian automatically includes all interactions necessary for a correct description of the internal dynamics.

Calculated dipole moments of ketenimine and its isotopologues are listed in **Table 3**. Our DMS yields equilibrium dipole moments for the main ketenimine isotopologue of $^a\mu_e = 0.5008$ D and $^c\mu_e = 1.4056$ D, where superscripts a and c refer to the principal axis components of the dipole vector $\vec{\mu}_e$. Symmetric H/D substitution results in a rotation of the a- and c- axis around the b axis. As a consequence, the components $^a\mu_e$ and $^c\mu_e$ of the dipole vector differ among the ketenimine isotopologues but the total dipole moment of $|\vec{\mu}_e| = 1.4912$ D is unchanged. The situation is different for the ground state dipole moments $\vec{\mu}_0$ due to variations of vibrational averaging effects. Overall, vibrational averaging results in a lowering of both a- and c-axis components. The non-deuterated isotopologue shows slightly larger effects due to vibrational averaging, especially for the c-axis component. Rodler et al. (1984) determined the dipole vector components of

the main isotopologue and from Stark shifts of the $2_{02} \leftarrow 1_{01}$ and $2_{11} \leftarrow 1_{10}$ rotational transitions. While the resulting $^c\mu_0 = 1.371(6)$ D is in excellent agreement with our calculated value of 1.3766 D, a somewhat larger difference is observed between the experimental $^a\mu_0 = 0.431(1)$ D and calculated 0.4587 D. This difference is in part due to a geometric effect. Using the optimized ae-CCSD(T)-F12b/CVTZ-F12 geometry, equilibrium dipole moments of $^a\mu_e = 0.4854$ D (-0.0154 D) and $^c\mu_e = 1.4029$ D (-0.0027 D) were obtained from DCSD/VTZ-F12 calculations, where values in parentheses correspond to the difference with respect to the values quoted in **Table 3**. Adding the vibrational averaging correction yields an approximate $^a\mu_0 \approx 0.4433$ D, closer to the experimental result. Again, the influence of high-order coupled-cluster terms would be required to further reduce the remaining error.

3.2. Vibrational Spectrum

The purely vibrational transitions of ketenimine and its isotopologues are listed in **Table 4**. Clearly, for the deuterated species the majority of experimental assignments is missing and a comparison of the different experimental results for H_2CCNH shows that these results bear an uncertainty of several wavenumbers.

Concerning the assignments for the non-deuterated ketenimine, a huge difference of more than 80 cm^{-1} between the computed and experimental values of Bane et al. (2011c) can be seen for mode ν_4. An analysis showed that this mode shows a strong Fermi resonance with the overtone of ν_7 and our calculated value of 1350.9 cm^{-1} for $2\nu_7$ agrees nicely with the experimental value of 1355 cm^{-1}. As our calculations clearly assign the transition at 1435.9 cm^{-1} to the fundamental mode, we believe that the experimental value of 1355 cm^{-1} belongs to the $2\nu_7$ overtone, which is the lower state of this Fermi pair. The reason for this misassignment might be that the infrared intensity of the overtone is much stronger than that for the fundamental. A closer look at this particular resonance reveals a peculiar feature. While the band intensity at the VSCF level amounts to 3.42 km/mol for ν_4 and 4.47 km/mol for $2\nu_7$, almost all intensity is transferred to the overtone within the VCI calculations. This can be understood by comparison to a VPT2 based analysis that accounts for the Fermi resonance (Vázquez and Stanton, 2007). Then, the intensities of the Fermi dyad in question are predominantly determined by the mixed a-axis transition dipole moments $\langle^a\mu\rangle_v$. The latter are obtained from the eigenvector components C_ω^v of the Fermi resonance matrix and the (deperturbed; dp) transition dipole moments $\langle^a\mu\rangle_\omega^{dp}$ evaluated over harmonic basis functions $|\omega\rangle$ according to:

$$\langle^a\mu\rangle_{\nu_4} = C_{\omega_4}^{\nu_4} \cdot \langle^a\mu\rangle_{\omega_4}^{dp} + C_{2\omega_7}^{\nu_4} \cdot \langle^a\mu\rangle_{2\omega_7}^{dp}$$
$$= 0.78 \cdot 0.033 \text{ D} + 0.62 \cdot -0.044 \text{ D} \approx 0.002 \text{ D}$$

and

$$\langle^a\mu\rangle_{2\nu_7} = C_{\omega_4}^{2\nu_7} \cdot \langle^a\mu\rangle_{\omega_4}^{dp} + C_{2\omega_7}^{2\nu_7} \cdot \langle^a\mu\rangle_{2\omega_7}^{dp}$$
$$= -0.62 \cdot 0.033 \text{ D} + 0.78 \cdot -0.044 \text{ D} \approx -0.055 \text{ D},$$

TABLE 4 | Comparison of calculated VCI fundamental frequencies of $H_2C=C=NH$ and its deuterated isotopologues with experimental data.

#	Sym.	$H_2C=C=NH$							$D_2C=C=ND$				$H_2C=C=ND$			
		Harm.	VCI	Int.	Exp.[a]	Exp.[b]	Exp.[c]	Exp.[d]	Harm.	VCI	Int.	Exp.[d]	Harm.	VCI	Int.[a]	Exp.[d]
ν_1	A′	3492.7	3315.4	10.9		3321.8			2563.0	2464.4	17.1		3177.1	3046.7	29.7	
ν_2		3177.0	3048.0	2.6					2325.3	2250.1	40.7	2246	2562.9	2467.4	20.1	
ν_3		2084.4	2041.8	281.9		2037	2043.6	2040	2044.1	1997.7	150.2	1998	2067.2	2027.7	287.0	2028
ν_4		1440.3	1435.9	0.1		1355			1231.5	1207.2	0.7		1440.2	1424.7	3.4	
ν_5		1140.1	1122.5	16.9		1127		1124	944.4	921.7	23.3	921	1136.0	1120.4	11.7	1120
ν_6		1045.1	1006.7	200.2	1000.2	1004	1000.2	1000	824.5	804.1	77.0	800	829.9	807.7	74.1	817
ν_7		705.5	691.1	77.2	692.9			690	555.3	549.6	39.8		705.2	679.5	53.4	693
ν_8		463.3	464.3	19.8	466.5				417.6	415.5	27.0		427.9	426.5	24.0	
ν_9	A″	3276.2	3132.5	0.2					2441.0	2359.3	0.0		3276.4	3131.4	0.2	
ν_{10}		1000.3	980.7	0.6	983.1				842.2	831.0	0.0		1000.4	979.2	0.1	
ν_{11}		904.6	876.0	29.6		872		872	666.2	653.7	27.9	648	752.2	731.4	19.1	
ν_{12}		405.8	405.7	0.4	409.0				351.4	349.4	0.2		400.8	399.4	0.2	

Frequencies are given in cm^{-1} and infrared intensities in km/mol.
[a]*Experimental gas phase values taken from Bane et al. (2011c,c,a).*
[b]*Experimental values taken from the compilation in Bane et al. (2011c).*
[c]*Experimental values taken from Ito et al. (1990) and Ito and Nakanaga (2010).*
[d]*Experimental Ar matrix values taken from Jacox and Milligan (1963) and Jacox (1979).*

where the corresponding values have been inserted. As can be seen from above equations, the efficient intensity stealing results from a compensation of the signs of the eigenvectors and the deperturbed transition dipole moments. The analysis and composition of all observed resonances of the fundamental modes of all isotopologues based on VCI calculations is summarized in **Table 5**. For all other fundamental modes of the non-deuterated molecule the agreement of the VCI calculations with the experimental results is excellent and the maximum deviation is no larger than $6.2\,cm^{-1}$, which is within the error bar of potential energy surfaces obtained from explicitly correlated coupled-cluster theory (Rauhut et al., 2009). In order to reduce this remaining error even further one would need to incorporate a number of corrections within the electronic structure calculations as for example high-order coupled-cluster terms, core-correlation effects, relativistic contributions, etc. (Ruden et al., 2004; Meier et al., 2011).

The results for the fully deuterated isotopologue, i.e., D_2CCND are of the same quality as for H_2CCNH and thus the VCI results most likely provide reliable predictions for all fundamentals. Most remarkably for this isotopologue are the very strong intensities for ν_3 and its resonance partners (cf. **Table 5**). The results for H_2CCND look more inconsistent than for the other two isotopologues. While modes ν_3 and ν_5 are in excellent agreement with the experimental results, the VCI results for ν_6 and ν_7 deviate by 9.3 and $13.5\,cm^{-1}$ from the experimental reference data, respectively. According to our VCI calculation, ν_6 shows a weak Fermi resonance with the overtone of ν_{12} (due to its weak character it has not been listed in **Table 5**). As such coupling pairs are sensitive with respect to environmental effects as arising from the argon matrix, the deviation of $9.3\,cm^{-1}$ may be explained this way. However, we consider this rather unlikely, but suspect difficulties in pinpointing the transition energies in the experiment, because Jacox reports

that *overlapping parent molecule absorptions and unassigned contributions of other products such as the partially deuterated methyl cyanides complicate the assignment of other absorptions to the partially deuterated ketenimines* (Jacox, 1979). Note that for all isotopologues, ν_4 shows strong Fermi resonances, but with different partners and in all cases the intensity of the overtone is stronger than for the fundamental.

3.3. Rotational Spectrum

In **Figure 1**, our computed RVCI rotational spectrum of ketenimine (**Figure 1A**) is compared with a simulated experimental spectrum (**Figure 1B**) for a temperature of $T = 50$ K. The latter spectrum has been calculated with the SPCAT program (Pickett, 1991) using the spectroscopic parameters of Degli Esposti et al. (2014) determined from the submillimeter wave spectrum, while intensities are based on the experimentally determined dipole moments in the vibrational ground state (Rodler et al., 1984). Intensities are given relative to the strongest line at $T = 50$ K, which corresponds to the $5_{2,3} \rightarrow 6_{3,3}$ transition in both cases. Excellent agreement between the RVCI and the experimental spectrum is observed. Only very subtle frequency differences appear upon close inspection, which occur mainly due to the difference of about $0.3\,GHz$ in the employed A rotational constants (compare **Table 2**). The overall shape of the spectrum, which is dominated by $^cR_{10}$ branch progressions and the sharp ^cQ branches, is nicely reproduced by the RVCI spectrum.

We have studied the temperature dependence of the ground state rotational spectrum in the range 20 to 300 K and results are depicted in **Figure 2**. With increasing temperature the intensity of the rotational transitions decrease by about a factor of 2 and the rather sharp $^cQ_{10}$ branches below 600 GHz broaden significantly. While for $T = 20$ K the $^cR_{10}$ transitions originating in $K_a = 1$ states are the strongest up to 2 THz, with each

TABLE 5 | Resonances of the fundamental modes of ketenimine and its isotopologues.

Molecule	Mode	Freq.	Int.	Composition					
H_2CCNH	ν_4	1435.9	0.1	4^1	(55.8%)	7^2	(35.2%)		
		1350.9	8.4	7^2	(53.3%)	4^1	(36.1%)		
	ν_{11}	876.0	29.6	11^1	(59.6%)	$8^1 12^1$	(36.7%)		
		880.5	18.6	$8^1 12^1$	(57.1%)	11^1	(39.0%)		
D_2CCND	ν_4	1207.2	0.7	4^1	(69.9%)	$6^1 12^1$	(21.4%)		
		1220.6	1.9	$6^1 12^1$	(60.3%)	4^1	(25.6%)		
	ν_3	1997.7	150.2	3^1	(49.1%)	$4^1 6^1$	(24.8%)		
		2019.2	40.1	$4^1 6^1$	(52.3%)	$6^2 8^1$	(16.7%)	3^1	(13.3%)
		2001.0	136.6	$6^2 8^1$	(41.2%)	3^1	(42.0%)		
	ν_1	2464.4	17.1	1^1	(65.0%)	$6^1 10^2$	(27.5%)		
		2467.0	12.0	$6^1 10^2$	(55.2%)	1^1	(37.2%)		
H_2CCND	ν_5	1120.4	11.7	5^1	(50.9%)	$7^1 8^1$	(27.8%)	$11^1 12^1$	(16.8%)
		1108.1	8.1	$7^1 8^1$	(64.4%)	5^1	(28.9%)		
		1133.6	4.8	$11^1 12^1$	(77.1%)	5^1	(15.8%)		
	ν_4	1424.7	3.4	4^1	(52.7%)	7^2	(28.5%)		
		1345.3	12.9	7^2	(57.8%)	4^1	(31.6%)		

Frequencies are given in cm^{-1} and infrared intensities in km/mol.
[1,2]*The superscripts denote the excitation levels of the individual modes.*
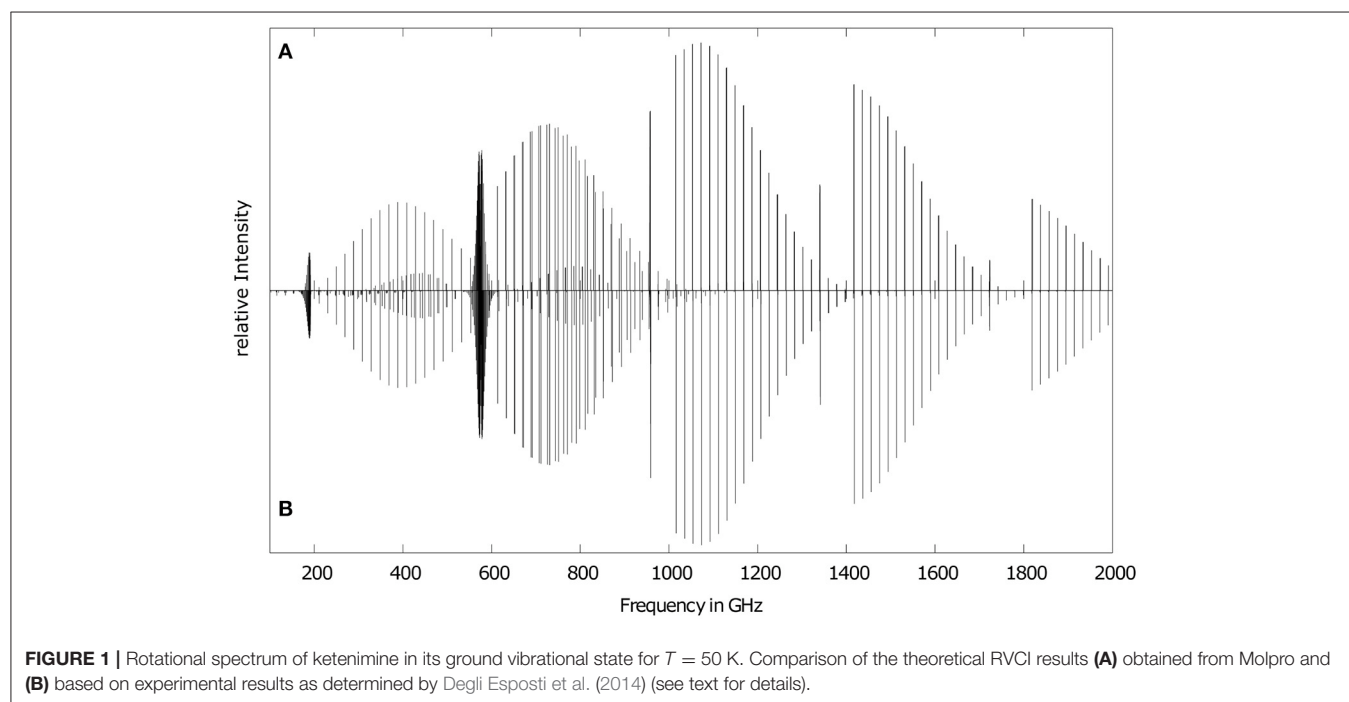
FIGURE 1 | Rotational spectrum of ketenimine in its ground vibrational state for $T = 50$ K. Comparison of the theoretical RVCI results **(A)** obtained from Molpro and **(B)** based on experimental results as determined by Degli Esposti et al. (2014) (see text for details).

increase in temperature the maximum shifts by one unit in K_a. Furthermore, the effect of asymmetry splitting in $K_a = 1$ states are clearly visible. All these observations originate in the Boltzmann distribution function resulting in a higher partition function and a shift in the thermal distribution toward higher K_a and J. The former is responsible for the emergence of higher energy branches and the latter for the shifts in the maximum for individual J-progressions, highlighting the importance of an accurate determination of the partition function.

3.4. Rovibrational Spectrum

It is known that the rovibrational spectrum of ketenimine shows many strongly coupled rovibrational bands in the energy regime between 300 and 1200 cm^{-1} (Bane et al., 2011a,b,c). For this reason, we want to give a broad overview over this area with **Figure 3**. The figure shows the 5 fundamental bands ν_5, ν_6, ν_7, ν_8, ν_{11}, as well as the overtone $2\nu_8$ and the combination band $\nu_{12} + \nu_8$. The comparison between RVCI and RCI spectra allows for a better understanding of the coupling and resonance
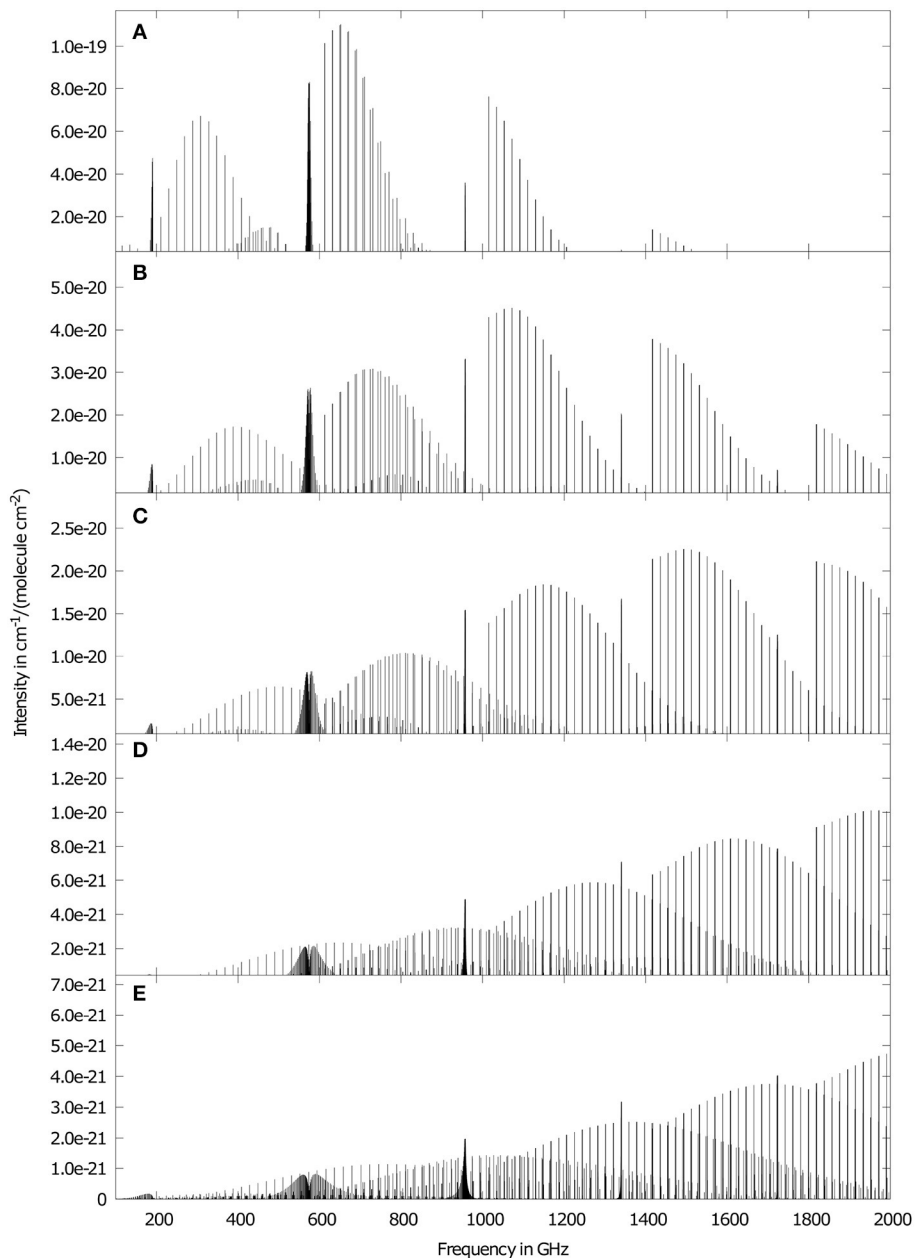
FIGURE 2 | Ground state rotational RVCI spectrum of ketenimine for different temperatures, **(A)** 20 K, **(B)** 50 K, **(C)** 100 K, **(D)** 200 K, **(E)** 300 K. Temperatures are considered only in the occupation numbers and not in line broadening. For the sake of clarity, the intensity axis of adjacent sub-figures are downscaled by a factor of two for increasing temperatures.

effects. Two examples for these couplings can be seen around 400 and 900 cm^{-1}. Therefore these areas are displayed in separate **Figures 4** and **5** and will be discussed below. For the following figures, we did not use any line broadening, since no direct comparison with experimental results is depicted.

A good example for the strong Coriolis-coupling in this system can be seen in **Figure 4** between ν_8 and ν_{12}. The bottom subplot (**Figure 4B**) shows the results of the RCI calculation, where Coriolis-coupling is not considered. ν_{12} has about two

orders of magnitude less intensity then ν_8, in line with the band intensities obtained from VCI (cf. **Table 4**). The in-plane CCN bending vibration ν_8 clearly shows an A-type spectrum, whereas the out-of-plane CCN bend ν_{12} shows the expected B-type intensity pattern. Inclusion of Coriolis-coupling in the upper subplot (**Figure 4A**) results in ν_{12} gaining about one order of magnitude in intensity by intensity borrowing in the RVCI calculation. The missing intensity in the stronger band is hard to see, since the relative difference is smaller. Furthermore, ν_{12}
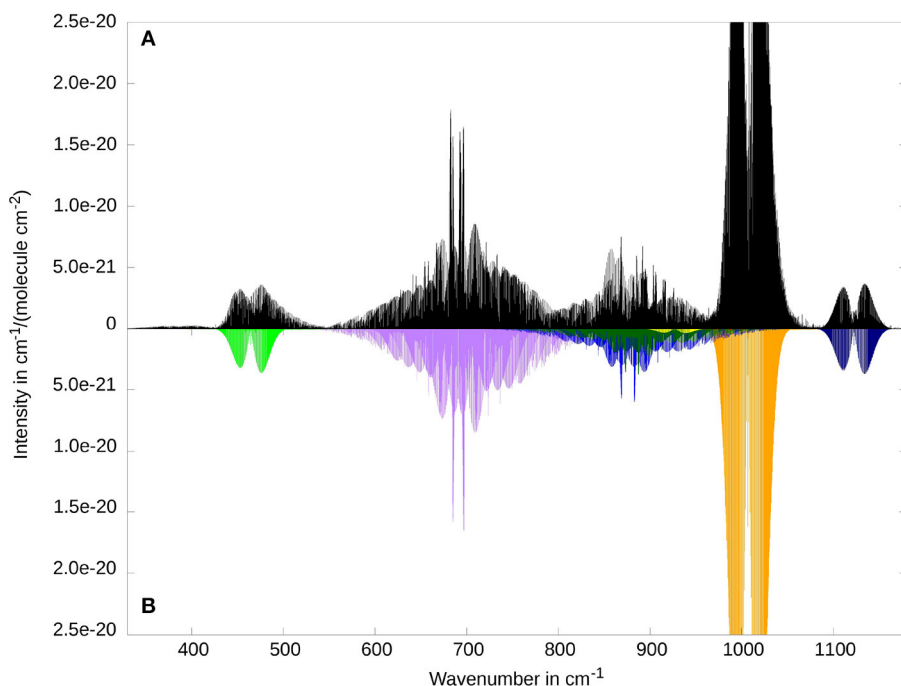
FIGURE 3 | Overview of the low frequency range of the rovibrational spectrum of ketenimine. Comparison between RVCI **(A)** and RCI **(B)** results. Visible contributions are provided by the fundamental bands ν_8 (at 464.4 cm^{-1}, CCN in-plane bend, in light green), ν_7 (at 691.2 cm^{-1}, CH$_2$ wagging, in purple), ν_{11} (at 876.2 cm^{-1}, torsion, in light blue), ν_6 (at 1007.1 cm^{-1}, CNH bend, in orange), ν_5 (at 1122.5 cm^{-1}, CCN stretch, in dark blue) as well as the combination band $\nu_8 + \nu_{12}$ (at 880.7 cm^{-1} in dark green), and the overtone $2\nu_8$ (at 927.3 cm^{-1} in yellow).
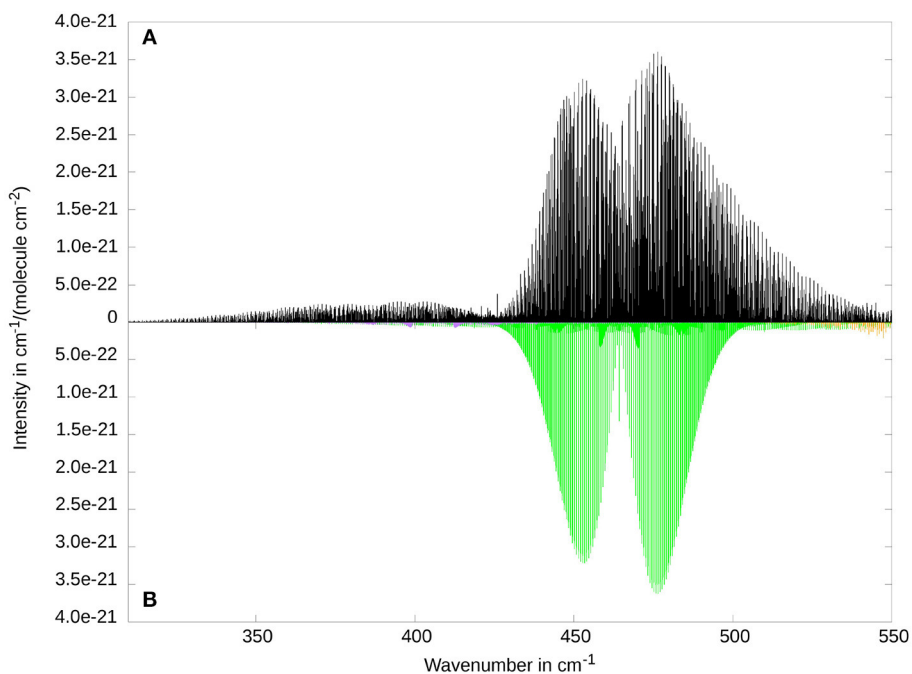
FIGURE 4 | The two lowest fundamental bands ν_{12} (at 405.7 cm^{-1}, CCN out-of-plane bend, VCI intensity 0.4 km/mol, in purple) and ν_8 (at 464.4 cm^{-1}, CCN in-plane bend, VCI intensity 19.8 km/mol, in light green) as well as small contributions of ν_7 (at 691.2 cm^{-1}, CH$_2$ wagging, in orange). Comparison between RVCI **(A)** and RCI **(B)**.

FIGURE 5 | Rovibrational spectrum of ketenimine of the fundamental bands ν_7 (at 691.2 cm^{-1}, in purple), ν_{11} (at 876.2 cm^{-1}, in light blue), ν_{10} (at 980.7 cm^{-1}, in red, barely visible) and ν_6 (at 1007.1 cm^{-1} in orange) and the combination band $\nu_8 + \nu_{12}$ (at 880.7 cm^{-1} in dark green), and the overtone $2\nu_8$ (at 927.3 cm^{-1} in yellow). Comparison between RVCI **(A)** and RCI **(B)** results.
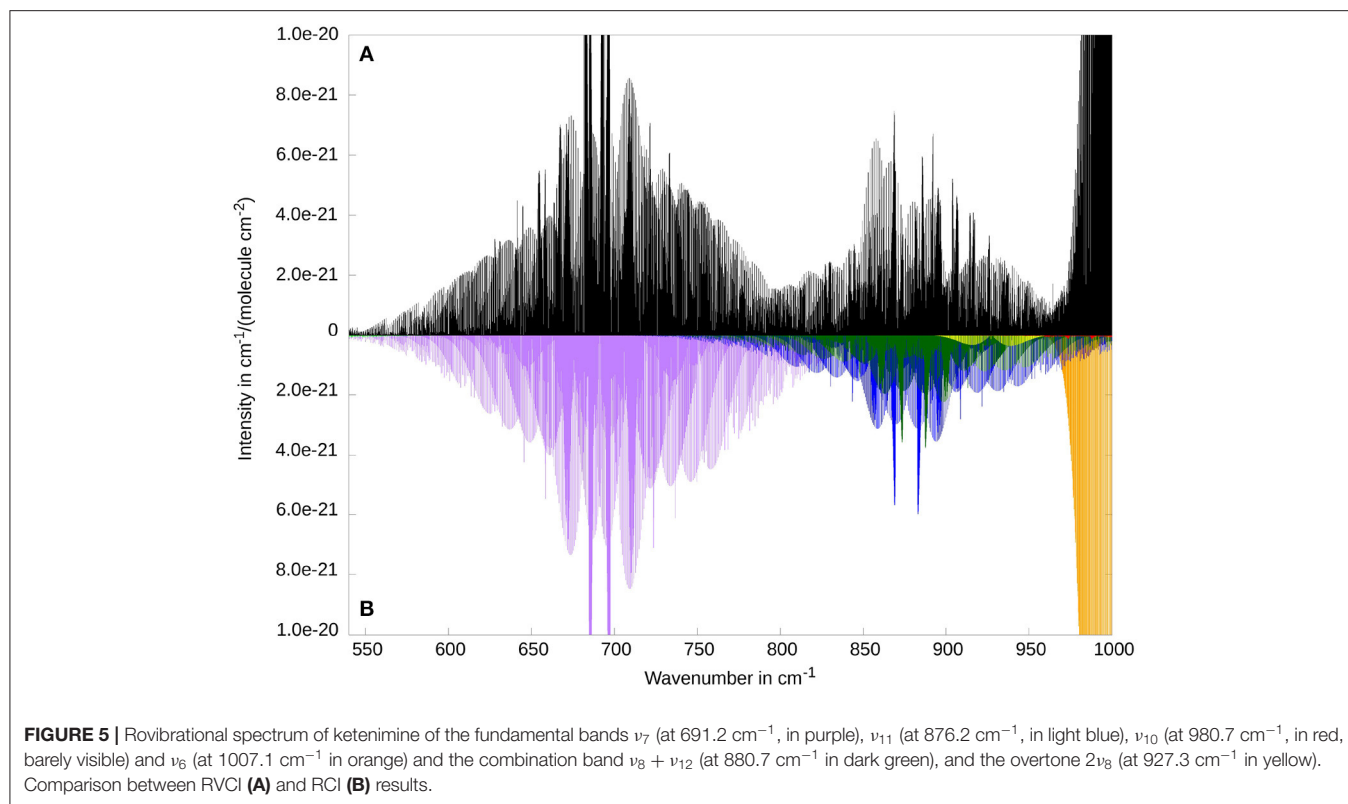
can neither be assigned to an A-type nor a B-type band structure, due to the lifting of the typical selection rules via Coriolis-coupling. For the ν_8 fundamental, the overall shape of an A-type transition is retained. Both bands show a rather asymmetric structure, with a supposed band center of the ν_{12} mode shifted by about 20 cm^{-1} to lower energies and visible transitions well below 350 cm^{-1}. This is in contrast to ν_8, where both branches gain intensity toward higher energies, with an overlapping region at about 470 cm^{-1}. The high energy tails of the R-branch (around 530 cm^{-1}) could also be influenced by the ν_7 mode (orange in **Figure 4**). However, we expect that effect to be small, since the VCI energies of the two modes ν_7 and ν_8 are separated by more than 200 cm^{-1}.

A comparison with the experimental and simulated spectra of Bane and coworkers (Figures 2A and B in Bane et al., 2011c) shows in general good agreement for ν_{12} (**Figure 4** as well as in **Supplementary Figure 1**). This holds for both the number of progressions and their distribution over the spectral range from 330 to 410 cm^{-1}. However, there seems to be a sudden drop in intensity at 410 cm^{-1} that can not be found in our calculated results. The slight shift of our RVCI-spectrum by about 4 cm^{-1} compared to experiment can be explained by our error in the VCI energy of 3.3 cm^{-1} (cf. **Table 4**). Comparing the spectra of Bane et al. for ν_8 (Figures 2C and D in Bane et al., 2011c) with ours (compare also in **Supplementary Figure 2**) shows somewhat larger deviations. While the A-type P and R branch structure is still recognizable in **Figure 4**, the spectra of Bane et al. show a broader distribution of the K_a sub-bands leading to the A-type band shape being partially obscured. It

should be mentioned that there are isolated peaks protruding both bands (see Bane et al., 2011c). Tests have shown (see **Supplementary Figures 1–4**) that such prominent peaks as well as the above discussed differences in the intensity patterns originate from line broadening. Since we do not use any broadening, those protruding peaks cannot be expected in our spectrum, but of course must appear in the experimental spectra.

In contrast to the previously considered modes, the CH$_2$ wagging mode ν_7 does not change its macroscopic shape due to Coriolis coupling. As can be seen in **Figure 5**, the general form of ν_7 corresponds to a C-type transition of a near-prolate asymmetric top molecule. The main difference due to RVCI (in the top panel) is the splitting of the central Q-branches. In comparison with the work of Bane et al. (Figure 2B in Bane et al., 2011b), there are two small deviations besides the overall good agreement (compare also in **Supplementary Figure 3**). First, there is a small shift for the two high peaks in the middle of the mode. Second, the experiment seems to show a sudden drop in intensity between the middle (650 and 730 cm^{-1}) and the outer parts of the progression (above 730 and 650 cm^{-1}). As mentioned before, the distributed peaks shown in the paper of Bane et al. (2011b), are caused by a Gauss broadening of the experimental results and are therefore not to be expected in our spectra. The possible coupling of ν_7 with higher energy modes (above 750 cm^{-1} in **Figure 5**) is not shown in the simulated spectrum of Bane et al. (2011b).

Another example of extensive rovibrational coupling occurs between 780 and 970 cm^{-1} (see **Figure 5**). The reason for
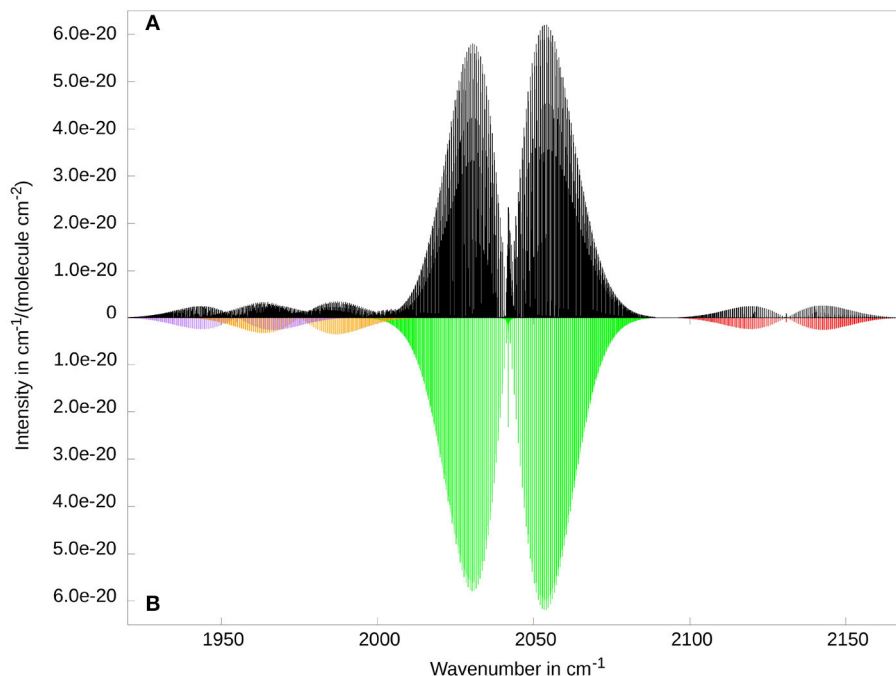
FIGURE 6 | Rovibrational spectrum of ketenimine in the region of the strongest fundamental band ν_3 (at 2041.8 cm^{-1}, CCN stretch, in green). Additionally, the overtones $2\nu_{10}$ (at 1955.0 cm^{-1}, in purple), and $2\nu_6$ (at 1975.1 cm^{-1}, in orange), as well as the combination band $\nu_5 + \nu_6$ (at 2130.8 cm^{-1}, in red) provide visible contributions in this spectral range. Comparison between RVCI **(A)** and RCI **(B)** results.

this is the close proximity of three vibrational bands: one fundamental band (ν_{11} at 876.2 cm^{-1}, torsion, A'' symmetry), one combination band ($\nu_8 + \nu_{12}$ at 880.7 cm^{-1}, A'' symmetry) and one overtone ($2\nu_8$ at 927.3 cm^{-1}, A' symmetry) within 50 cm^{-1}. Additionally, there is a further "dark state" involved, corresponding to the overtone of the out-of-plane CCN bending mode ($2\nu_8$ at 809.6 cm^{-1}, A' symmetry). While the overtones $2\nu_{12}$ and $2\nu_8$ are strongly coupled to the combination band $\nu_8 + \nu_{12}$ via a-axis Coriolis-coupling ($\zeta_{8,12}^a = -0.802$), similar to the correspondingly coupled fundamentals, the ν_{11} fundamental has been shown to be in Fermi resonance with the combination band (cf. **Table 5**). The resulting rovibrational coupling leads to an almost complete loss of discernible band structure when comparing the RCI (bottom panel) and the RVCI spectrum (top panel). As a consequence, experimental assignment and interpretation of this spectral region will be highly difficult without reliable estimates of spectroscopic parameters obtained from theory.

Figure 6 reveals only very weak Coriolis coupling between ν_3 and $2\nu_6$, respectively $2\nu_{10}$. One reason for this is that the largest non-vanishing ζ constants for $\zeta_{3,6}^\alpha$ and $\zeta_{3,10}^\alpha$ correspond to b and c direction, respectively. Hence the rotational constants along the b and c direction have to be considered. Since they are a factor of 20 smaller then the A rotational constant, the coupling is significantly weaker. In addition to that, Coriolis coupling between a fundamental band and the overtone of another band requires at least the first order in the $\boldsymbol{\mu}$-tensor expansion. Therefore, it is possible that in experiments a somewhat stronger

coupling occurs, even though it is unlikely due to the small rotational constants. The only experimental results for this mode have been presented by Ito et al. (1990). While a direct comparison of spectra is ambiguous, due to relatively low resolution and a contamination of the experimental probe, Ito et al. do note signs of Coriolis perturbations in the fitted effective spectroscopic parameters of the ν_3 band.

Figure 7 shows the XH stretching fundamental region between 3000 and 3500 cm^{-1}. The corresponding fundamental bands are the symmetric (ν_2) and antisymmetric (ν_9) CH$_2$ stretch vibrations and the NH stretching mode (ν_1), in energetically ascending order. Additionally, the $\nu_3 + \nu_5$ and the $\nu_3 + \nu_6$ combination bands provide a significant contribution to the spectrum. All bands show the expected shapes of A-type (ν_2, $\nu_3 + \nu_5$, and $\nu_3 + \nu_6$), B-type (ν_1), and C-type (ν_9) transitions. So far there were no experimental results published for any of these bands. The comparison between RCI (bottom) and RVCI results (top) gives no indications for substantial Coriolis coupling among the fundamental bands. This is supported by taking the corresponding Coriolis coupling constants into account, where the largest (absolute) value is found for $\zeta_{2,9}^c \approx 0.05$. Due to the restriction to a constant $\boldsymbol{\mu}$-tensor, no direct Coriolis coupling between fundamentals ν_i and combination bands $\nu_j + \nu_k$ is included in the RVCI-matrix. While a strong interaction between ν_2 and $\nu_3 + \nu_5$ is unlikely because of very small ζ-constants ($|\zeta_{2j}^b| \approx 0.003$), such a coupling might be relevant for the ν_9 fundamental due to the close by $\nu_3 + \nu_6$ combination band and the substantial intensity difference. However, experimental
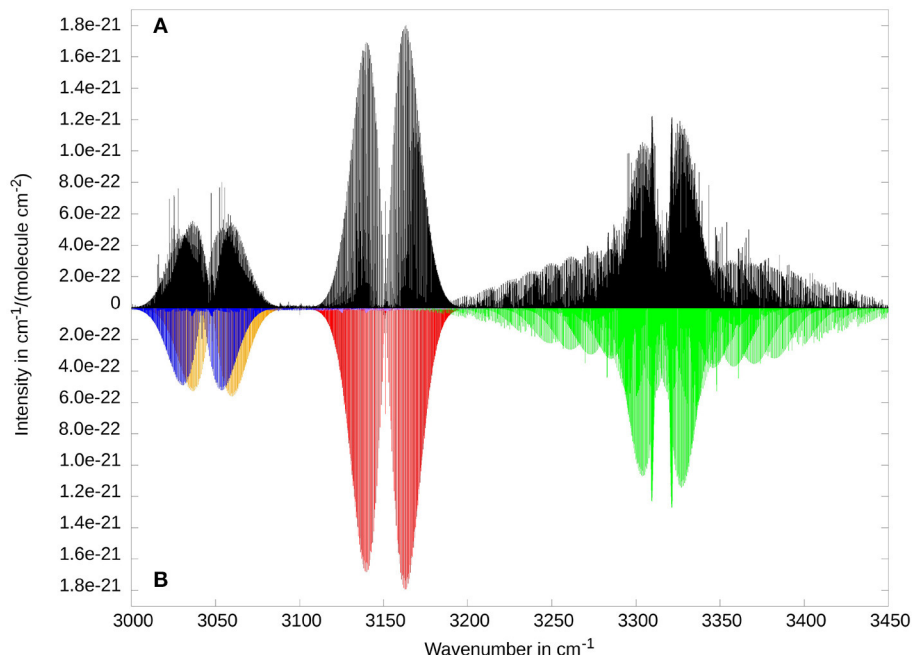
FIGURE 7 | Rovibrational spectrum of ketenimine in the region of XH stretching fundamentals. Three fundamental bands ν_2 (at 3048.0 cm^{-1}, symmetric CH$_2$ stretch, in orange), ν_9 (at 3132.5 cm^{-1}, anti-symmetric CH$_2$ stretch, in purple, barely visible) and ν_1 (at 3315.4 cm^{-1}, NH stretch, in light green) are shown, as well as the combination bands $\nu_3 + \nu_5$ (at 3042.0 cm^{-1}, in blue) and $\nu_3 + \nu_6$ (at 3151.1 cm^{-1} in red). Comparison between RVCI **(A)** and RCI **(B)** results.

observation of ν_9 will be complicated by the fact that ν_9 rovibrational transitions will most likely be hidden in between the stronger $\nu_3 + \nu_6$ band. Overall the rovibrational transitions in this spectral region have rather low intensity compared to other spectral regions. The VCI band intensity of the strongest vibrational transition ν_1 (10.9 km/mol) is already a factor of about 20 lower than the two strongest fundamental bands (cf. **Table 4**).

3.5. Summary and Conclusions

The vibrational, rotational and rovibrational spectra of ketenimine have been studied by high-level *ab initio* methods for the first time. Based on a new series of almost black-box algorithms being implemented in the MOLPRO package of quantum chemical programs, it was possible to simulate and analyze the complex rovibrational features of this near-prolate asymmetric top molecule. Note, that the input information for these calculations comprises just the molecular structure and the call of the requested modules, which act in a highly optimized—with respect to memory requirements and CPU time—and automated manner. Agreement with available experimental data, i.e., ground state rotational constants, vibrational band origins, dipole moments or the rotational spectrum as a whole, was found to be excellent or at least very good. Beside the reliable reproduction of experimental reference data, many predictions could be provided, which we consider a trustworthy guidance for new experimental studies or astrochemical observations. The occurrence of several Fermi resonances even for fairly low lying transitions requested accurate potential energy and dipole

surfaces, which has been accomplished by explicitly correlated coupled-cluster theory and the rather new distinguishable clusters approximation. A proper description of these resonances was found to be important for the subsequent rovibrational calculations. For example, the strong Fermi resonance of mode ν_{11} with the combination band $\nu_8 + \nu_{12}$ has significant impact on the spectrum, but was not discussed in the experimental work (Bane et al., 2011a). This example demonstrates the benefits, that can arise from combined experimental and theoretical studies to provide reliable reference data for astrophysical studies. Covering a wide spectral range and identifying signature areas within the spectrum are challenging goals in the future. Currently, work is in progress to include coupling terms originating from higher-order $\boldsymbol{\mu}$-tensor terms and hot bands.

DATA AVAILABILITY STATEMENT

The original contributions generated for the study are included in the article/**Supplementary Material**, further inquiries can be directed to the corresponding author/s.

AUTHOR CONTRIBUTIONS

MT performed all RVCI calculations, generated all figures, and wrote parts of the text. GR supervised the project, performed the VCI calculations, and wrote parts of the text. SE wrote large parts of the program being used for producing the data. BS performed VCI and RCI calculations, analyzed the spectra, and wrote parts

of the text. All authors contributed to the article and approved the submitted version.

SUPPLEMENTARY MATERIAL

The Supplementary Material for this article can be found online at: https://www.frontiersin.org/articles/10.3389/fchem.2020.623641/full#supplementary-material

REFERENCES

Adler, T. B., Knizia, G., and Werner, H.-J. (2007). A simple and efficient CCSD(T)-F12 approximation. *J. Chem. Phys.* 127:221106. doi: 10.1063/1.2817618

Alajarin, M., Marin-Luna, M., and Vidal, A. (2012). Recent highlights in ketenimine chemistry. *Eur. J. Org. Chem.* 2012, 5637–5653. doi: 10.1002/ejoc.201200383

Aliev, M. R., and Watson, J. K. G. (1985). "Chapter 1 - Higher-order effects in the vibration-rotation spectra of semirigid molecules," in *Molecular Spectroscopy: Modern Research, Vol. 3*, ed K. N. Rao (Orlando, FL: Academic Press), 1–67. doi: 10.1016/B978-0-12-580643-5.50006-3

Allamandola, L. J., Tielens, A. G. G. M., and Barker, J. R. (1989). Interstellar polycyclic aromatic hydrocarbons: the infrared emission bands, the excitation/emission mechanism, and the astrophysical implications. *Astrophys. J. Suppl. Ser.* 71:733. doi: 10.1086/191396

August, J. (1986). Spectroscopic studies of nitriles, enimines and ynamines of importance in interstellar chemistry. Ph.D. thesis. Sussex University.

Ball, J. A., Gottlieb, C. A., Lilley, A. E., and Radford, H. E. (1970). Detection of methyl alcohol in sagittarius. *Astrophys. J.* 162:L203. doi: 10.1086/180654

Bane, M. K., Robertson, E. G., Thompson, C. D., Appadoo, D. R. T., and McNaughton, D. (2011a). High-resolution Fourier-transform infrared spectroscopy of the ν_6 and Coriolis perturbation allowed $\nu_1 0$ modes of ketenimine. *J. Chem. Phys.* 135:224306. doi: 10.1063/1.3664624

Bane, M. K., Robertson, E. G., Thompson, C. D., Medcraft, C., Appadoo, D. R. T., and McNaughton, D. (2011b). High-resolution Fourier-transform infrared spectroscopy of the Coriolis coupled ground state and ν_7 mode of ketenimine. *J. Chem. Phys.* 134:234306. doi: 10.1063/1.3597775

Bane, M. K., Thompson, C. D., Robertson, E. G., Appadoo, D. R. T., and McNaughton, D. (2011c). High-resolution FTIR spectroscopy of the ν_8 and Coriolis perturbation allowed $\nu_1 2$ bands of ketenimine. *Phys. Chem. Chem. Phys.* 13, 6793–6798. doi: 10.1039/C0CP01816C

Brown, R., Rice, E., and Rodler, M. (1985). *Ab initio* studies of the structures and force fields of ketenimine and related molecules. *Chem. Phys.* 99, 347–356. doi: 10.1016/0301-0104(85)80175-0

Cami, J., Bernard-Salas, J., Peeters, E., and Malek, S. E. (2010). Detection of $C_6 0$ and $C_7 0$ in a Young Planetary Nebula. *Science* 329, 1180–1182. doi: 10.1126/science.1192035

Carvalho, G. A., and Pilling, S. (2020). Photolysis of CH_3CN Ices by soft X-rays: implications for the chemistry of astrophysical ices at the surroundings of X-ray sources. *J. Phys. Chem. A* 124, 8574–8584. doi: 10.1021/acs.jpca.0c06229

Charbonneau, D., Brown, T. M., Noyes, R. W., and Gilliland, R. L. (2002). Detection of an extrasolar planet atmosphere. *Astrophys. J.* 568:377. doi: 10.1086/338770

Czakó, G., Mátyus, E., and Császár, A. G. (2009). Bridging theory with experiment: a benchmark study of thermally averaged structural and effective spectroscopic parameters of the water molecule. *J. Phys. Chem. A* 113, 11665–11678. doi: 10.1021/jp902690k

Degli Esposti, C., Dore, L., and Bizzocchi, L. (2014). Accurate rest-frequencies of ketenimine (CH_2CNH) at submillimetre wavelength. *Astron. Astrophys.* 565:A66. doi: 10.1051/0004-6361/201423589

Dinu, D. F., Ziegler, B., Podewitz, M., Liedl, K. R., Loerting, T., Grothe, H., et al. (2020). The interplay of VSCF/VCI calculations and matrix-isolation IR spectroscopy-Mid infrared spectrum of CH_3CH_2F and CD_3CD_2F. *J. Mol. Spectrosc.* 367:111224. doi: 10.1016/j.jms.2019.111224

Endres, C. P., Schlemmer, S., Schilke, P., Stutzki, J., and Müller, H. S. P. (2016). The cologne database for molecular spectroscopy, CDMS, in the virtual atomic and molecular data centre, VAMDC. *J. Mol. Spectrosc.* 327, 95–104. doi: 10.1016/j.jms.2016.03.005

Erfort, S., Tschöpe, M., and Rauhut, G. (2020a). Toward a fully automated calculation of rovibrational infrared intensities for semi-rigid polyatomic molecules. *J. Chem. Phys.* 152:244104. doi: 10.1063/5.0011832

Erfort, S., Tschöpe, M., Rauhut, G., Zeng, X., and Tew, D. P. (2020b). Ab initio calculation of rovibrational states for non-degenerate double-well potentials: cis-trans isomerization of HOPO. *J. Chem. Phys.* 152:174306. doi: 10.1063/5.0005497

Gandhi, S., Brogi, M., Yurchenko, S. N., Tennyson, J., Coles, P. A., Webb, R. K., et al. (2020). Molecular cross-sections for high-resolution spectroscopy of super-Earths, warm Neptunes, and hot Jupiters. *Mon. Not. R. Astron. Soc.* 495, 224–237. doi: 10.1093/mnras/staa981

Godfrey, P. D., Brown, R. D., Robinson, B. J., and Sinclair, M. W. (1973). Discovery of Interstellar Methanimine (Formaldimine). *Astrophys. Lett.* 13:119.

Herbst, E., and van Dishoeck, E. F. (2009). Complex organic interstellar molecules. *Annu. Rev. Astron. Astrophys.* 47, 427–480. doi: 10.1146/annurev-astro-082708-101654

Hill, J. G., Mazumder, S., and Peterson, K. A. (2010). Correlation consistent basis sets for molecular core-valence effects with explicitly correlated wave functions: the atoms B-Ne and Al-Ar. *J. Chem. Phys.* 132:054108. doi: 10.1063/1.3308483

Ito, F., and Nakanaga, T. (2010). Observation of the high-resolution spectrum of the N-H bending vibration of ketenimine CH_2CNH. *J. Mol. Spectrosc.* 264, 100–104. doi: 10.1016/j.jms.2010.09.012

Ito, F., Nakanaga, T., Sugawara, K.-i., Takeo, H., Sugie, M., Matsumura, C., et al. (1990). Observation of the High-Resolution Infrared Spectrum of the ν_4 Band of Ketenimine, CH_2CNH. *J. Mol. Spectrosc.* 140, 177–184. doi: 10.1016/0022-2852(90)90016-J

Jacox, M. E. (1979). Matrix isolation study of the interaction of excited argon atoms with methyl cyanide, vibrational and electronic spectra of ketenimine. *Chem. Phys.* 43, 157–172. doi: 10.1016/0301-0104(79)85184-8

Jacox, M. E., and Milligan, D. E. (1963). Infrared study of the reactions of CH_2 and NH with C_2H_2 and C_2H_4 in solid argon. *J. Am. Chem. Soc.* 85, 278–282. doi: 10.1021/ja00886a006

Jefferts, K. B., Penzias, A. A., and Wilson, R. W. (1970). Observation of the CN radical in the orion nebula and W51. *Astrophys. J.* 161:L87. doi: 10.1086/180576

Kaneti, J., and Nguyen, M. T. (1982). Theoretical study of ketenimine: geometry, electronic properties, force constants and barriers to inversion and rotation. *J. Mol. Struct.* 87, 205–210. doi: 10.1016/0166-1280(82)80054-7

Kats, D., Kreplin, D., Werner, H.-J., and Manby, F. R. (2015). Accurate thermochemistry from explicitly correlated distinguishable cluster approximation. *J. Chem. Phys.* 142:064111. doi: 10.1063/1.4907591

Kats, D., and Manby, F. R. (2013). The distinguishable cluster approximation. *J. Chem. Phys.* 139:021102. doi: 10.1063/1.4813481

Kawaguchi, K., Takano, S., Ohishi, M., Ishikawa, S.-I., Miyazawa, K., Kaifu, N., et al. (1992). Detection of HNCCC in TMC-1. *Astrophys. J.* 396:L49. doi: 10.1086/186514

Knizia, G., and Werner, H.-J. (2008). Explicitly correlated RMP2 for high-spin open-shell reference states. *J. Chem. Phys.* 128:154103. doi: 10.1063/1.2889388

Krim, L., Guillemin, J., and Woon, D. (2019). Formation of methyl ketenimine ($CH_3CH=C=NH$) and ethylcyanide ($CH_3CH_2C\equiv N$) isomers through successive hydrogenations of acrylonitrile ($CH_2 \quad =CH\text{-}C\equiv N$) under interstellar conditions: the role of $CH_3C^\bullet H\text{-}C\equiv N$ radical in the activation of the cyano group chemistry. *MNRAS* 485, 5210–5220. doi: 10.1093/mnras/stz698

Lovas, F., Hollis, J., Remijan, A., and Jewell, P. (2006). Detection of ketenimine (CH_2CNH) is Sagittarius B2(N) hot cores. *Astrophys. J.* 645, L137–L140. doi: 10.1086/506324

Mandell, A. M., Haynes, K., Sinukoff, E., Madhusudhan, N., Burrows, A., and Deming, D. (2013). Exoplanet transit spectroscopy using wfc3: Wasp-12 b, wasp-17 b, and wasp-19 b. *Astrophys. J.* 779:128. doi: 10.1088/0004-637X/779/2/128

Martín-Pintado, J., de Vicente, P., Wilson, T. L., and Gaume, R. (1996). "A hot ring in the Sgr B2 molecular cloud," in *Science With Large Millimetre Arrays*, ed P. A. Shaver (Berlin; Heidelberg: Springer Berlin Heidelberg), 210–213. doi: 10.1007/978-3-540-69999-6_30

McGuire, B. A. (2018). 2018 census of interstellar, circumstellar, extragalactic, protoplanetary disk, and exoplanetary molecules. *Astrophys. J. Suppl. Ser.* 239:17. doi: 10.3847/1538-4365/aae5d2

Meier, P., Neff, M., and Rauhut, G. (2011). Accurate vibrational frequencies of borane and its isotopologues. *J. Chem. Theory Comput.* 7, 148–152. doi: 10.1021/ct1004752

Müller, H. S. P., Schlöder, F., Stutzki, J., and Winnewisser, G. (2005). The cologne database for molecular spectroscopy, CDMS: a useful tool for astronomers and spectroscopists. *J. Mol. Struct.* 742, 215–227. doi: 10.1016/j.molstruc.2005.01.027

Müller, H. S. P., Thorwirth, S., Roth, D. A., and Winnewisser, G. (2001). The cologne database for molecular spectroscopy, CDMS. *Astron. Astrophys.* 370, L49-L52. doi: 10.1051/0004-6361:20010367

Neff, M., Hrenar, T., Oschetzki, D., and Rauhut, G. (2011). Convergence of vibrational angular momentum terms within the Watson Hamiltonian. *J. Chem. Phys.* 134:064105. doi: 10.1063/1.3551513

Neff, M., and Rauhut, G. (2009). Toward large scale vibrational configuration interaction calculations. *J. Chem. Phys.* 131:124129. doi: 10.1063/1.3243862

Öberg, K. I. (2016). Photochemistry and astrochemistry: photochemical pathways to interstellar complex organic molecules. *Chem. Rev.* 116, 9631–9663. doi: 10.1021/acs.chemrev.5b00694

Ohishi, M. (2019). "Prebiotic complex organic molecules in space," in *Astrobiology: From the Origins of Life to the Search for Extraterrestrial Intelligence*, eds A. Yamagishi, T. Kakegawa, and T. Usui (Singapore: Springer Singapore), 11–21. doi: 10.1007/978-981-13-3639-3_2

Ohishi, M., and Kaifu, N. (1998). Chemical and physical evolution of dark clouds - Molecular spectral line survey toward TMC-1. *Faraday Discuss.* 109, 205–216. doi: 10.1039/a801058g

Papoušek, D., and Aliev, M. R. (1982). *Molecular Vibrational-rotational Spectra: Theory and Applications of High Resolution Infrared, Microwave and Raman Spectroscopy of Polyatomic Molecules*. Elsevier Science Ltd.

Petrenko, T., and Rauhut, G. (2017). A new efficient method for the calculation of interior eigenpairs and its application to vibrational structure problems. *J. Chem. Phys.* 146:124101. doi: 10.1063/1.4978581

Pflüger, K., Paulus, M., Jagiella, S., Burkert, T., and Rauhut, G. (2005). Multi-level vibrational SCF calculations and FTIR measurements on Furazan. *Theor. Chem. Acc.* 114, 327–332. doi: 10.1007/s00214-005-0678-4

Pickett, H. M. (1991). The fitting and prediction of vibration-rotation spectra with spin interactions. *J. Mol. Spectrosc.* 148, 371–377. doi: 10.1016/0022-2852(91)90393-O

Puzzarini, C., Salta, Z., Tasinato, N., Lupi, J., Cavallotti, C., and Barone, V. (2020). A twist on the reaction of the CN radical with methylamine in the interstellar medium: new hints from a state-of-the-art quantum-chemical study. *MNRAS* 496, 4298–4310. doi: 10.1093/mnras/staa1652

Rauhut, G. (2015). Anharmonic Franck-condon factors for the $\tilde{X}^2B_1 \leftarrow \tilde{X}^1A_1$ photoionization of ketene. *J. Phys. Chem. A* 119, 10264–10271. doi: 10.1021/acs.jpca.5b06922

Rauhut, G., Knizia, G., and Werner, H.-J. (2009). Accurate calculation of vibrational frequencies using explicitly correlated coupled-cluster theory. *J. Chem. Phys.* 130:054105. doi: 10.1063/1.3070236

Rodler, M., Brown, R. D., Godfrey, P. D., and Kleinbömer, B. (1986). The rotation-inversion spectrum of ketenimine, $H_2C=C=NH$. *J. Mol. Spectrosc.* 118, 267–276. doi: 10.1016/0022-2852(86)90240-7

Rodler, M., Brown, R. D., Godfrey, P. D., and Tack, L. M. (1984). Generation, microwave spectrum and dipole moment of ketenimine. *Chem. Phys. Lett.* 110, 447–451. doi: 10.1016/0009-2614(84)87068-2

Ruden, T. A., Helgaker, T., Jørgensen, P., and Olsen, J. (2004). Coupled-cluster connected quadruples and quintuples corrections to the harmonic vibrational frequencies and equilibrium bond distances of HF, N2, F2, and CO. *J. Chem. Phys.* 121, 5874–5884. doi: 10.1063/1.1780155

Špirko, V., Jensen, P., Bunker, P., and Čejchan, A. (1985). The development of a new Morse-oscillator based rotation-vibration Hamiltonian for H_3^+. *J. Mol. Spectrosc.* 112, 183–202. doi: 10.1016/0022-2852(85)90203-6

Theule, P., Borget, F., Mispelaer, F., Danger, G., Duvernay, F., Guillemin, J. C., et al. (2011). Hydrogenation of solid hydrogen cyanide HCN and methanimine CH_2NH at low temperature. *Astron. Astrophys.* 534:A64. doi: 10.1051/0004-6361/201117494

Vasconcelos, F., Pilling, S., Agnihotri, A., Rothard, H., and Boduch, P. (2020). Methylenimine and cyanomethanimine synthesis from ion irradiation of N2-CH4 ice: implication on the formation of prebiotic molecules in outer solar system bodies. *Icarus* 351:113944. doi: 10.1016/j.icarus.2020.113944

Vázquez, J., and Stanton, J. F. (2007). Treatment of Fermi resonance effects on transition moments in vibrational perturbation theory. *Mol. Phys.* 105, 101–109. doi: 10.1080/00268970601135784

Wang, S. C. (1929). On the asymmetrical top in quantum mechanics. *Phys. Rev.* 34, 243–252. doi: 10.1103/PhysRev.34.243

Watson, J. K. G. (1968). Simplification of the molecular vibration-rotation Hamiltonian. *Mol. Phys.* 15, 479–490. doi: 10.1080/00268976800101381

Watson, J. K. G. (1977). "Aspects of quartic and sextic centrifugal effects on rotational energy levels," in *Vibrational Spectra and Structure, Vol. 6*, ed J. R. Durig (Amsterdam: Elsevier), 1–89.

Weinreb, S., Barrett, A. H., Meeks, M. L., and Henry, J. C. (1963). Radio observations of OH in the interstellar medium. *Nature* 200, 829–831. doi: 10.1038/200829a0

Werner, H.-J., Knowles, P., Manby, F., Black, J., Doll, K., Heßelmann, A., et al. (2020). The Molpro quantum chemistry package. *J. Chem. Phys.* 152:144107. doi: 10.1063/5.0005081

Wilson, R. W., Jefferts, K. B., and Penzias, A. A. (1970). Carbon monoxide in the orion nebula. *Astrophys. J.* 161:L43. doi: 10.1086/180567

Woon, D. E. (2002). Pathways to glycine and other amino acids in ultraviolet-irradiated astrophysical ices determined via quantum chemical modeling. *Astrophys. J.* 571, L177-L180. doi: 10.1086/341227

Yagi, K., Hirata, S., and Hirao, K. (2007). Multiresolution potential energy surfaces for vibrational state calculations. *Theor. Chem. Acc.* 118, 681–691. doi: 10.1007/s00214-007-0363-x

Zaleski, D. P., Seifert, N. A., Steber, A. L., Muckle, M. T., Loomis, R. A., Corby, J. F., et al. (2013). Detection of E-cyanomethanimine toward sagittarius B2(N) in the green bank telescope PRIMOS survey. *Astrophys. J. Lett.* 765:L10. doi: 10.1088/2041-8205/765/1/L10

Ziegler, B., and Rauhut, G. (2016). Efficient generation of sum-of-products representations of high-dimensional potential energy surfaces based on multimode expansions. *J. Chem. Phys.* 144:114114. doi: 10.1063/1.4943985

Ziegler, B., and Rauhut, G. (2018). Rigorous use of symmetry within the construction of multidimensional potential energy surfaces. *J. Chem. Phys.* 149:164110. doi: 10.1063/1.5047912